INTERNATIONAL JOURNAL FOR NUMERICAL METHODS IN FLUIDS
Int. J. Numer. Meth. Fluids 2000; **33**: 559–581

A boundary-only approach to the deformation of a shear-thinning drop in extensional Newtonian flow

Roger E. Khayat*,[1]

Department of Mechanical and Materials Engineering, Faculty of Engineering Science, The University of Western Ontario, London, Ontario, Canada

SUMMARY

The influence of shear thinning on drop deformation is examined through a numerical simulation. A two-dimensional formulation within the scope of the boundary element method (BEM) is proposed for a drop driven by the ambient flow inside a channel of a general shape, with emphasis on a convergent–divergent channel. The drop is assumed to be shear thinning, obeying the Carreau–Bird model and the suspending fluid is Newtonian. The viscosity of the drop at any time is estimated on the basis of a rate-of-strain averaged over the region occupied by the drop. The viscosity thus changes from one time step to the next, and it is strongly influenced by drop deformation. It is found that small drops, flowing on the axis, elongate in the convergent part of the channel, then regain their spherical form in the divergent part; thus confirming experimental observations. Newtonian drops placed off-axis are found to rotate during the flow with the period related to the initial extension, i.e. to the drop aspect ratio. This rotation is strongly prohibited by shear thinning. The formulation is validated by monitoring the local change of viscosity along the interface between the drop and the suspending fluid. It is found that the viscosity averaged over the drop compares, generally to within a few per cent, with the exact viscosity along the interface. Copyright © 2000 John Wiley & Sons, Ltd.

KEY WORDS: boundary element; drop deformation; Newtonian flow; shear thinning

1. INTRODUCTION

This paper examines the effect of shear thinning on drop deformation in confined low-Reynolds number flow. The study focuses on the interplay between shear and elongation effects on drop deformation in a convergent–divergent channel. The problem is of industrial and academic interest as it is related to the mixing, dispersion and compounding of polymer blends. A shear- or elongation-dominated drop deformation depends on the size of the drop relative to the channel dimension(s), and its position relative to the axis of the channel. With

* Correspondence to: Department of Mechanical and Materials Engineering, Faculty of Engineering Science, The University of Western Ontario, London, Ontario, Canada N6A 5B9.
[1] E-mail: rkhayat@eng.uwo.ca

Received 12 August 1998
Revised 19 August 1999

regard to mixing, the dominance of shear or elongation is crucial to understand. The preparation of polymer blends requires the mechanical mixing of at least two macromolecular species and additives to achieve optimal morphology. Most blends are prepared in either a single- or a twin-screw extruder, where the flow is dominated by shear. Mixing in the shear field can be deficient. To generate the same deformation in shear flow, a greater amount of energy is required than in extensional flow. More importantly, shear flow is incapable of dispersing liquids that are four times more viscous than the matrix liquid. The extensional flow is also more efficient for generating the dispersive as well as the distributive mixing [1].

Although favourable conditions for efficient mixing have been well established, understanding the mechanism leading to the successful implementation of these conditions has not been achieved; optimization of the geometry and processing conditions remain heavily dependent on empiricism. Several factors are known to affect the quality of mixing in the convergent–divergent flow. They include the flow rate of fluid through the channel, the initial drop diameter, the ratio of extensional viscosities of drop and suspending fluid, the channel convergence length-to-diameter ratio, the angle of convergence, the viscoelastic character of both fluids, the magnitude of the imposed stresses, the shear thinning character of both fluids, the relative magnitude of the shear and extensional flow fields, the number of passages through the convergence and their separation. These factors affect both the dispersive and distributive mixings. Given the multi-parameter nature of the problem, it is difficult to rely solely on empirical means to achieve optimal mixing; for this reason, theoretical modelling would be highly desirable. Since drop deformation in a confined or unconfined medium represents a problem of the moving boundary type, the boundary element method (BEM) becomes ideally suited for the treatment of this problem.

The deformation of neutrally buoyant viscous drops at low Reynolds number has received considerable attention (see Rallison [2] and Stone [3] for reviews). While extensive work has been devoted to the modelling and simulation of drops deforming in an infinite fluid medium, relatively little results have been reported for a drop deforming in a confined medium. Recently [4–8], the influence of shear and elongation on the deformation of a drop in two-dimensional channels has been examined using the BEM for Newtonian [4,5] and viscoelastic systems [6–8]. The formulation was applied for drop deformation problems in convergent–divergent and purely convergent channels [4,6–8], and the overflight region of a mixing extruder [5]. Experiments were carried out in a rectangular channel for drops initially located on or off the tube axis. Good agreement was obtained upon comparison between theory and experiment despite the limiting assumption of two-dimensional analysis [7,8]. The influence of shear and elongation was examined as the drop deformed inside the channel. The influence of viscosity ratio and interfacial tension on drop deformation was also examined [4–8]. Some of the work focused on the drop deformation as affected by the converging flow in channels of different geometry. The deformation of initially non-circular drops was also examined.

The BEM relates velocities at points within the fluid to the velocity and stress on the boundary. It is thus an ideal method for studying moving boundary problems, where the velocity on the moving interface or free surface is the quantity of prime interest. The advantages of the BEM include the reduction of problem dimension, the direct calculation of the interfacial velocity, the ability of the method to track large interfacial deformations, and

the potential for easy incorporation of interfacial tension, as well as other surface effects. The present paper is part of a series of studies on the applicability of the BEM to problems of the moving boundary type. Such problems include the planar deformation of a drop in a confined medium [4–8], gas-assisted injection moulding [9], air venting during blow moulding and thermoforming [10] and the transient mixing of Newtonian and viscoelastic fluids [11,12]. In particular, Khayat [13] proposed first an Eulerian BEM approach for free surface and interface problems. The approach is based on the discretization of the whole cavity similarly to the finite element method (FEM). In this case, the BEM loses its main advantage since domain discretization is needed. Later, Khayat and Marek [14] developed an adaptive (Lagrangian) BEM for confined (cavity) flow with a free surface. The method takes full advantage of the BEM as only the boundary is meshed (and remeshed with time).

The inherent transient nature of these flow processes, and the presence of a moving interface or free surface, make the simulation challenging because of the non-linearities involved [15]. The challenge becomes even greater if additional non-linearities, such as those stemming form non-Newtonian effects, are included [16]. Traditionally, when the BEM is used, non-Newtonian terms are considered as a pseudo-body force [17–20]. The resulting boundary integral equation includes a volume integral involving the body force, which requires the discretization of the inner domain of computation into internal cells over which the volume integral is evaluated. The BEM thus loses its main advantage relative to conventional volume methods, as it ceases to be a boundary-only approach. More recent techniques, such as the methods of dual and multiple reciprocity BEMs, have been developed to transform the volume integral into a boundary integral [21–25]. Although these methods still require the evaluation of the flow field at internal points, they do not require the discretization of the inner domain, and the BEM retains its major advantage. However, the ability of such techniques to handle highly non-linear problems remains questionable.

For non-linear moving domain problems, the implementation of the BEM is even more difficult than for problems with fixed domain. This is precisely the case of a shear-thinning drop deforming in a confined or infinite medium. The implementation of a boundary-only scheme is difficult due to the non-linear dependence of viscosity on the rate-of-strain tensor. The volume integral that includes the non-linear term may be evaluated through a discretization of the flow domain. However, unlike non-linear problems over a fixed domain, the drop must be remeshed because of the distortion of the cell elements, if a Lagrangian approach is used. This remeshing requirement adds considerably to the CPU and storage cost. Toose *et al.* [26] examined the two-dimensional deformation of a viscoelastic drop in an infinite viscous Newtonian fluid using inner-domain discretization. The corresponding axisymmetric problem was also tackled by Toose *et al.* [27]. Although the work of Toose *et al.* includes non-linear viscoelastic effects, it is restriction to a drop of constant viscosity, an infinite medium for the suspending fluid, and, most importantly, volume discretization is needed since a domain BEM is used. This method can be reasonably effective for simple problems, such as a drop deforming in an infinite medium. However, for complex configurations, such as the deformation of a drop in a confined medium, the deformation of two or more interacting drops, the very large deformation and break-up of a drop, the coalescence of two drops and three-dimensional deformation, the domain BEM becomes severely restrictive. Most of these situations are extremely difficult to deal with unless a boundary-only formulation can be implemented.

In the present work, the influence of shear thinning is examined for a drop deforming in a convergent–divergent channel using a boundary-only formulation. The boundary integral formulation is greatly simplified by estimating the viscosity of the drop on the basis of magnitude of the strain rate averaged over the region occupied by the drop. In this case, the domain integral is transformed into a surface integral. The boundary element formulation is presented in Section 2, where basic equations, boundary conditions, a summary of the derivation of the generalized Newtonian boundary integral equation and solution procedure are covered. Numerical assessment and computational results are covered in Section 3. The effects of drop size and initial position on deformation are closely examined in this study. Finally, Section 4 is devoted to a discussion on the validity of the proposed approximation for viscosity and some concluding remarks.

2. BOUNDARY ELEMENT FORMULATION

In this section, a generalized formulation of the boundary integral equations is derived for the deformation of a shear-thinning drop in a confined Newtonian medium. Both suspending fluid and drop are assumed to be viscous and incompressible. In the present case, the fluids of interest are typical polymers of high viscosity, subjected to small strain rates during processing. Thus, only low Reynolds number flow, typically characterized by small velocities, small length scales and/or high viscosity, will be considered. In this limit, inertia is negligible; the two-phase system is in a state of creeping motion.

2.1. Governing equations

At any instant t, the drop, which occupies a region $\Omega_d(t)$, is assumed to be neutrally buoyant, so the effects of gravity and any external body forces are neglected. The suspending fluid, which occupies the outer region $\Omega_s(t)$, is driven by an imposed pressure gradient. The regions $\Omega_s(t)$ and $\Omega_d(t)$ are assumed separated at all time by a moving interface $\Gamma_i(t)$ between them. Thus, situations where the drop comes in contact with the boundary of the channel, Γ_c, or breaks into two are excluded. Figure 1 illustrates schematically the general flow configuration and notations used. The region $\Omega_s(t)$ is always bounded by $\Gamma_i(t)$ and Γ_c. The conservation of mass and momentum equations in each region may be written as

$$\nabla \cdot \mathbf{u}_\alpha(\mathbf{x}, t) = 0, \qquad \nabla \cdot \boldsymbol{\sigma}_\alpha(\mathbf{x}, t) = \mathbf{0}, \qquad \mathbf{x} \in \Omega_\alpha(t) \cup \Gamma_\alpha(t) \tag{1}$$

with the subscript $\alpha = \mathrm{d}$ or s, corresponding to a variable in the drop or suspending fluid region, respectively. Here ∇ is the gradient operator, $\mathbf{x}$ is the position vector, $\mathbf{u}_\alpha(\mathbf{x}, t)$ is the velocity vector and $\boldsymbol{\sigma}_\alpha(\mathbf{x}, t)$ is the total stress tensor. For a generalized Newtonian fluid, the total stress tensor is given by $\boldsymbol{\sigma}_\alpha(\mathbf{x}, t) = -p_\alpha(\mathbf{x}, t)\mathbf{I} + \eta_\alpha(\mathbf{x}, t)\dot{\boldsymbol{\gamma}}_\alpha(\mathbf{x}, t)$, where the rate-of-strain tensor is expressed in terms of the velocity gradient and its transpose, and is equal to $\dot{\boldsymbol{\gamma}}_\alpha(\mathbf{x}, t) = \nabla \mathbf{u}_\alpha(\mathbf{x}, t) + \nabla \mathbf{u}_\alpha^t(\mathbf{x}, t)$, $p_\alpha(\mathbf{x}, t)$ is the hydrostatic pressure, $\mathbf{I}$ is the unit tensor and $\eta_\alpha(\mathbf{x}, t)$ is the viscosity of the fluid occupying region $\Omega_\alpha(t)$.

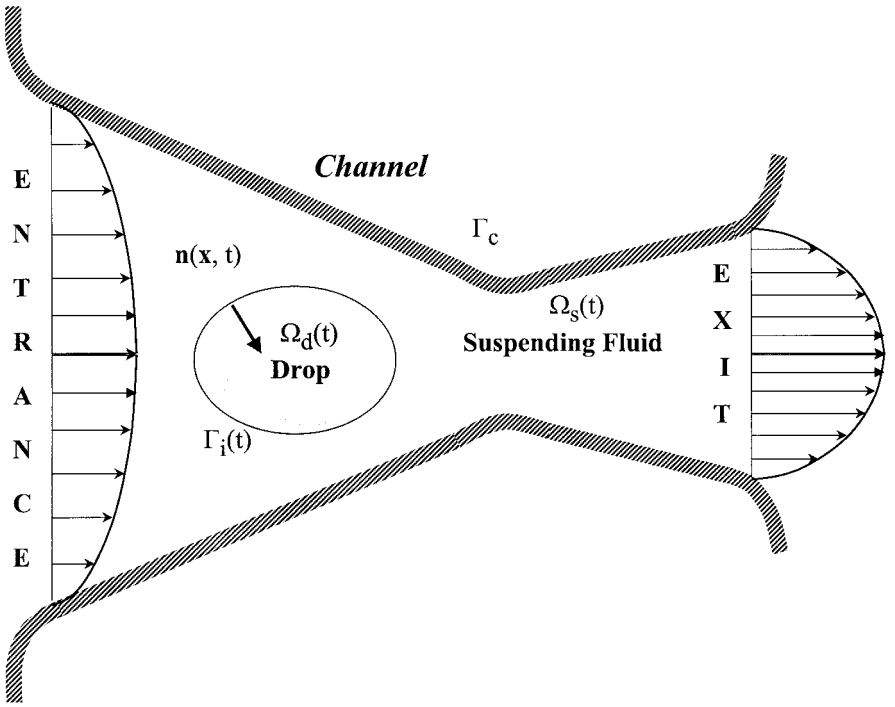

Figure 1. Schematic illustration of general flow configuration and notations.

In this work, the suspending fluid is assumed to be Newtonian so that η_s is constant. The drop is assumed to be shear thinning, with its viscosity obeying the four-parameter Carreau–Bird model [20]. In this case

$$\frac{\eta_d(\mathbf{x}, t) - \eta_d^\infty}{\eta_d^0 - \eta_d^\infty} = [1 + \lambda_d^2 |\dot{\gamma}_d(\mathbf{x}, t)|^2]^{(n-1)/2} \tag{2}$$

where η_d^0 is the zero shear rate viscosity, η_d^∞ is the infinite shear rate viscosity, λ_d is a time constant and n is the power-law exponent. Here $|\dot{\gamma}_\alpha(\mathbf{x}, t)|$ is the magnitude of the rate-of-stain tenor [20].

2.2. Boundary and initial conditions

The fluid is assumed to adhere to the solid boundary, so that stick and no-penetration conditions apply on Γ_c. Thus, the velocity is assumed to be fully prescribed on Γ_c, including the entrance and exit of the channel, where, for simplicity, the fluid is assumed to obey Poiseuille flow. Compactly, one may write

$$\mathbf{u}(\mathbf{x}, t) = \mathbf{u}_c(\mathbf{x}), \quad \mathbf{x} \in \Gamma_c \tag{3}$$

In principle, channel flow conditions must be applied for a flow between two flat plates, which is not exactly the situation at the entrance and exit of the channel in Figure 1. The present calculations and results are meant to illustrate the applicability of the proposed formulation. Other more realistic geometries and boundary conditions can be readily accommodated.

The interface is assumed to deform pointwise along the normal, $\mathbf{n}(\mathbf{x}, t)$, with the normal projection of the fluid velocity at the interface. This method keeps the points evenly distributed on the interface. Thus, the following kinematic boundary condition holds on $\Gamma_i(t)$:

$$\frac{d\mathbf{x}}{dt} = \mathbf{n}(\mathbf{x}, t)[\mathbf{n}(\mathbf{x}, t) \cdot \mathbf{u}_i(\mathbf{x}, t)], \quad \mathbf{x} \in \Gamma_i(t) \tag{4}$$

where $\mathbf{u}_i(\mathbf{x}, t)$ is the velocity at the interface. Here $\mathbf{n}$ is directed from the suspending fluid region to the region occupied by the drop. A Lagrangian approach, such as the one involving the solution of Equation (4), requires usually remeshing or mesh refinement of the free surface. Remeshing is relatively easily handled by the BEM, given the lower dimension of the boundary compared with that of the FEM.

The dynamic conditions at the interface are based on the continuity of the tangential stress and discontinuity of normal stress caused by the interfacial tension. Let $\mathbf{t}_\alpha(\mathbf{x}, t) = \boldsymbol{\sigma}_\alpha(\mathbf{x}, t) \cdot \mathbf{n}(\mathbf{x}, t)$ be the traction so that the dynamic condition becomes

$$\mathbf{t}_s(\mathbf{x}, t) - \mathbf{t}_d(\mathbf{x}, t) = v\mathbf{n}(\mathbf{x}, t)\nabla \cdot \mathbf{n}(\mathbf{x}, t), \quad \mathbf{x} \in \Gamma_i(t) \tag{5a}$$

Here v is the interfacial tension coefficient. The continuity of velocity also applies at the interface so that

$$\mathbf{u}_s(\mathbf{x}, t) = \mathbf{u}_d(\mathbf{x}, t) \equiv \mathbf{u}_i(\mathbf{x}, t), \quad \mathbf{x} \in \Gamma_i(t) \tag{5b}$$

As to the initial conditions, the fluid is assumed to be initially at rest; the fluid is in a stress free state.

2.3. Boundary integral equations and time marching scheme

The basic assumption adopted in the derivation of the boundary integral equations consists of taking the viscosity of the drop to be uniform over the drop region. However, the viscosity still depends on the rate-of-strain of the local flow as dictated by Equation (2). In this case, the integral equations for the two-fluid system remain the same form as that corresponding to Newtonian fluids. The derivation of the equations is thus similar to that in Reference [4]. Here, only the final results of the formulation are given as well as additional details for the determination of the rate-of-strain dependent viscosity of the drop.

For any fluid of time-dependent viscosity, $\eta_\alpha(t)$, occupying a region, $\Omega_\alpha(t) \cup \Gamma_\alpha(t)$, the generalized boundary integral equation is of the form

$$\frac{1}{\eta_\alpha(t)}\int_{\Gamma_\alpha(t)}\mathbf{t}(\mathbf{y},t)\cdot\mathbf{J}(\mathbf{x}|\mathbf{y})\,d\Gamma_\mathbf{y}-\int_{\Gamma_\alpha(t)}\mathbf{n}(\mathbf{y},t)\cdot\mathbf{u}_\alpha(\mathbf{y},t)\cdot\mathbf{K}(\mathbf{x}|\mathbf{y})\,d\Gamma_\mathbf{y}=c_\alpha(\mathbf{x},t)\mathbf{u}(\mathbf{x},t) \tag{6}$$

for $x\in\Omega_\alpha(t)\cup\Gamma_\alpha(t)$, where the function $c_\alpha(\mathbf{x},t)$ depends on time since the domain occupied by the fluid changes with time. Its value is equal to 1 for a point inside the domain. The kernels, or Green's functions, **J** and **K** are second and third rank tensors respectively and are the same as for Stokes flow [4,5].

The traction at the interface is eliminated by using condition (5a). After some manipulation, the integral equation for a point on the interface reads [4]

$$\begin{aligned}&\int_{\Gamma_i(t)}\left\{R_\eta(t)\mathbf{u}_i(\mathbf{y},t)\cdot\mathbf{n}(\mathbf{y},t)\cdot\mathbf{K}(\mathbf{x}|\mathbf{y})+\frac{v}{\eta_s}[\nabla_\mathbf{y}\cdot\mathbf{n}(\mathbf{y},t)]\mathbf{n}(\mathbf{y},t)\cdot\mathbf{J}(\mathbf{x}|\mathbf{y})\right\}d\Gamma_\mathbf{y}\\&+\int_{\Gamma_c}\left[\mathbf{u}_c(\mathbf{y})\cdot\mathbf{n}(\mathbf{y})\cdot\mathbf{K}(\mathbf{x}|\mathbf{y})-\frac{1}{\eta_s}\mathbf{t}_c(\mathbf{y},t)\cdot\mathbf{J}(\mathbf{x}|\mathbf{y})\right]d\Gamma_\mathbf{y}=c_d(\mathbf{x},t)\mathbf{u}_i(\mathbf{x},t),\quad\mathbf{x}\in\Gamma_i(t)\end{aligned} \tag{7}$$

Another integral equation is also needed, which relates the velocity and traction on the walls of the channel. It can be derived similarly to read

$$\begin{aligned}&[R_\eta(t)-1]\int_{\Gamma_i(t)}[\mathbf{u}_i(\mathbf{y},t)\cdot\mathbf{n}(\mathbf{y},t)\cdot\mathbf{K}(\mathbf{x}|\mathbf{y})]\,d\Gamma_\mathbf{y}\\&-\int_{\Gamma_c}\left[\mathbf{u}_c(\mathbf{y})\cdot\mathbf{n}(\mathbf{y})\cdot\mathbf{K}(\mathbf{x}|\mathbf{y})-\frac{1}{\eta_s}\mathbf{t}_c(\mathbf{y},t)\cdot\mathbf{J}(\mathbf{x}|\mathbf{y})\right]d\Gamma_\mathbf{y}=c_s(\mathbf{x},t)\mathbf{u}_c(\mathbf{x}),\quad\mathbf{x}\in\Gamma_c\end{aligned} \tag{8}$$

where the time-dependent viscosity ratio $R_\eta(t)$ has been introduced

$$R_\eta(t)=R_\eta^\infty+(R_\eta^0-R_\eta^\infty)[1+\lambda_d^2|\dot\gamma_d(t)|^2]^{(n-1)/2} \tag{9}$$

where $R_\eta^0=\eta_d^0/\eta_s$ and $R_\eta^\infty=\eta_d^\infty/\eta_s$. The rate-of-strain tenor is taken as the space average of $\dot\gamma_d(\mathbf{x},t)$ over the region $\Omega_d(t)\cup\Gamma_i(t)$

$$\begin{aligned}\dot\gamma_d(t)&\approx\frac{1}{S_d(t)}\int_{\Omega_d(t)}\dot\gamma_d(\mathbf{x},t)\,d\Omega_\mathbf{x}=\frac{1}{S_d(t)}\int_{\Omega_d(t)}[\nabla\mathbf{u}_d(\mathbf{x},t)+\nabla\mathbf{u}_d^t(\mathbf{x},t)]\,d\Omega_\mathbf{x}\\&=\frac{1}{S_d(t)}\int_{\Gamma_i(t)}[\mathbf{n}(\mathbf{x},t)\mathbf{u}_i(\mathbf{x},t)+\mathbf{u}_i(\mathbf{x},t)\mathbf{n}(\mathbf{x},t)]\,d\Gamma_\mathbf{x}\end{aligned} \tag{10}$$

where $S_d(t)$ is the area occupied by the drop. In this study, an explicit time marching scheme is used to update the interface and drop viscosity. In this case, the approximate evaluation of the rate-of-strain tensor given by Equation (10) becomes particularly convenient since the velocity $\mathbf{u}_i(\mathbf{x},t)$ at the interface is evaluated from the solution of Equations (7) and (8).

At each time step, $R_\eta(t)$ is known from the previous time step, and Equations (7) and (8) are solved similarly to the Newtonian problem as a coupled system. The integral equations (7) and (8) are discretized along $\Gamma_i(t)$ and Γ_c. The resulting algebraic system is solved to determine the velocity at the interface $\mathbf{u}_i(\mathbf{x},t)$ and the traction at the walls of the channel $\mathbf{t}_c(\mathbf{x}\in\Gamma_c,t)$. Also,

following the determination of these unknowns, the flow field off the interface and channel walls can be calculated using the appropriate equations in the drop region $\Omega_d(t)$ and the region $\Omega_s(t)$ occupied by the suspending fluid. The numerical solution of Equations (7) and (8) is obtained similarly to the Newtonian problem [4], and the simplest form of the BEM is adopted; the velocity and traction are assumed to be constant over each boundary element.

3. INFLUENCE OF SHEAR THINNING ON DROP DEFORMATION

In this section, the planar deformation of a shear-thinning drop is examined subject to the flow field of the suspending fluid inside a confining channel. Although the flow in channels of arbitrarily general geometry can be easily handled by the current formulation, here the emphasis is placed on (hyperbolic) convergent–divergent channels. The influence of ambient shear and elongation on drop deformation is examined. The deformation is also influenced by other material and geometric parameters, some of which have already been extensively studied elsewhere [4–6] and will not be covered here. The present study focuses mainly on the effect of shear thinning.

At time $t = 0$, the drop is assumed to be suddenly placed near the entrance to the channel, and subsequently subjected to the motion of the suspending fluid. Strictly speaking, the quasi-steady state hypothesis assumed in the formulation is not valid since the drop is subjected to a sudden acceleration at $t > 0$. But before examining the influence of the interplay between shear thinning and geometric aspects of the flow, it is important to assess the numerical accuracy of the formulation and algorithm described in the previous section.

3.1. Numerical assessment of convergence and accuracy

The convergence and accuracy of the present method can be assessed by monitoring the effects of the time increment and mesh size. A similar assessment was made for Newtonian [4] and linear viscoelastic [5] systems. Here only the effect of the time increment for a given mesh size will be studied by examining the motion of a shear-thinning drop moving along the axis of the convergent–divergent channel. The situation is typically shown in Figure 2. The length of the channel is equal to 20 cm, the entrance and exit widths are each equal to 14 cm and the neck width is 1.4 cm. For these and all subsequent calculations in this geometry, the number of boundary elements is fixed equal to 144 along the channel boundary and 144 along the drop/fluid interface. The relatively high number of elements along the interface is particularly necessary for drops undergoing large distortion. This mesh size is kept the same throughout the study. The value of the maximum velocity at the entrance is also fixed and is taken equal to 10 cm s^{-1}.

Consider now the situation depicted in Figure 2. The parameters in the Carreau–Bird model (7) are taken typically as for most materials of practical interest [20]. Throughout this study: $R_\eta^\infty = 0$ and $\lambda_d = 1$ s. For the drop in Figure 2, $R_\eta^0 = 5$ and $n = 0.6$. The influence of the time increment Δt on the numerical accuracy is shown in Figure 3 for $0.001 \leq \Delta t$ (s) ≤ 0.01, and an initial drop diameter $D_0 = 2$ mm. The evolution of the drop shape is shown in Figure 2 at various positions along the channel axis. The drop stretches in the converging flow region,

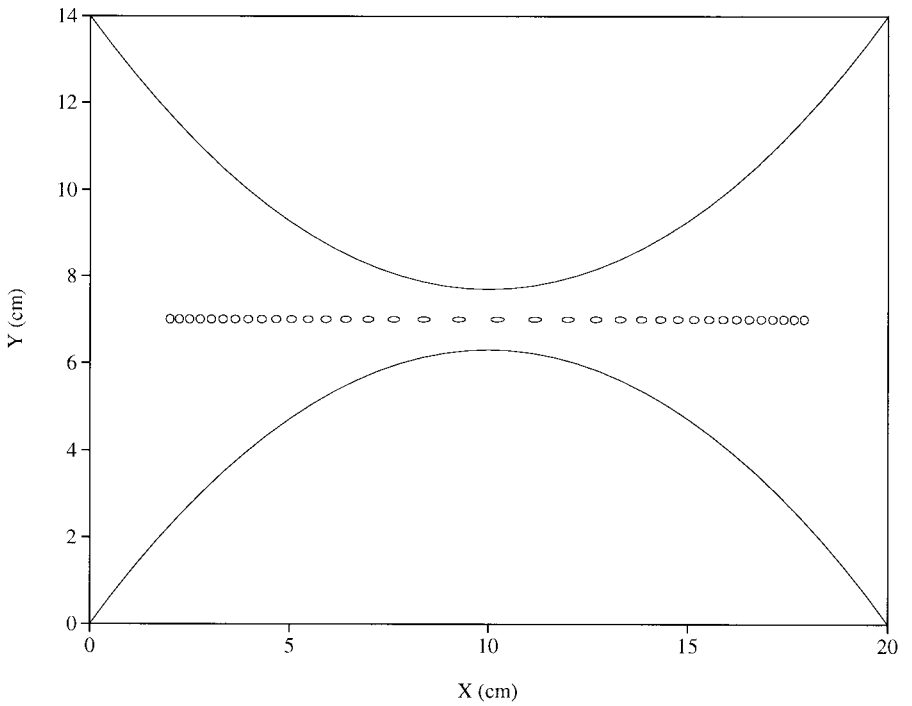

Figure 2. Typical drop deformation with initial diameter: $D_0 = 0.2$ cm flowing through a hyperbolic convergent–divergent flow channel. Dimensions are given in cm. The maximum flow velocity at the channel entrance is assumed: $\mathbf{u}_m = 10$ cm s^{-1}. In this case, $R_\eta^0 = 5$ and $n = 0.6$. The figure shows the channel geometry and drop deformation along channel axis.

reaches maximum elongation in the neck region, and recovers its initial (circular) shape as it nears the exit. In Figure 3 the evolution of the current-to-initial ratio of drop surface (volume), $S_d(t)/S_d^0$, is shown for three values of the time increment. The lack of surface (volume) conservation is a measure of numerical error. Generally, the error increases with time, reaches a maximum in the neck region and decreases again for any time increment. There is essentially no effect of Δt on the error before the drop reaches the neck region, at which point the rate of error increase is higher for the larger time increments. There is a rapid decrease of accuracy as the drop approaches the neck region and some levelling-off afterwards. Between the neck and the exit the rate of decrease of error is essentially the same. The error in all reported results in this paper was kept below 8%. To accomplish this accuracy, Δt was taken equal to at most 5 ms.

3.2. Influence of shear thinning

The influence of shear thinning on drop deformation is investigated by varying the power-law exponent n in Equation (9). The initial diameter of the drop is fixed at $D_0 = 4$ mm and the rest

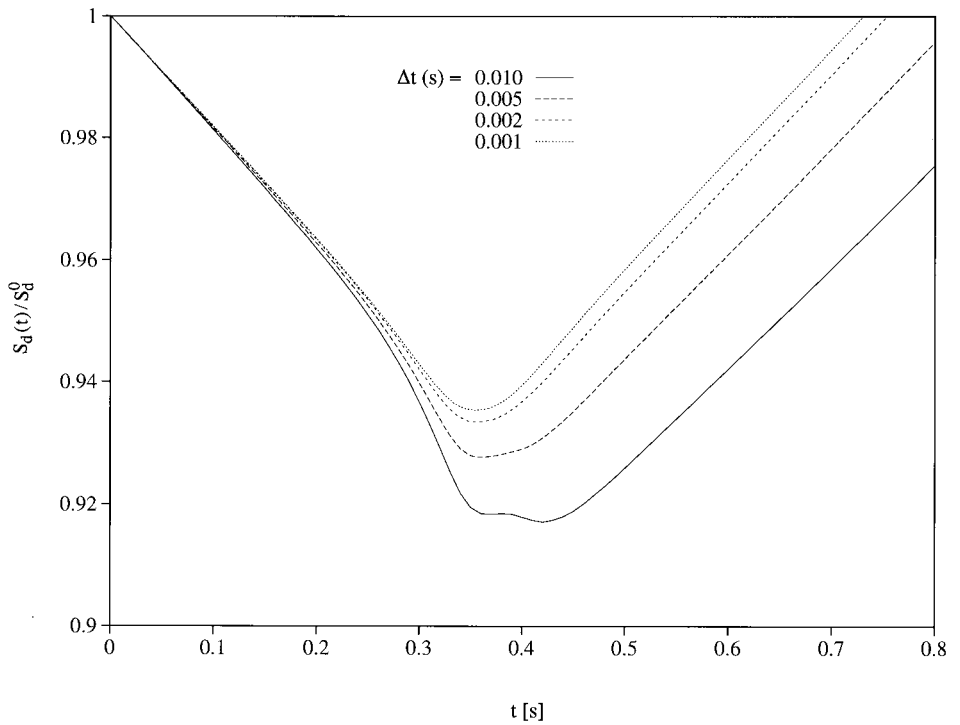

Figure 3. Influence of the time increment Δt on the error during drop deformation depicted in Figure 2. The evolution of the drop current-to-initial surface ratio, $S_d(t)/S_d^0$, is plotted for four time increments $0.001 \leq \Delta t \text{ (s)} \leq 0.01$ for the drop depicted in Figure 2.

of the parameters of the problem remain the same as before. Two main variables of interest are monitored, namely $R_\eta(t)$ and the relative deformation of the drop, $d(t)$, which is taken as the relative change of the current perimeter of the drop with respect to the initial perimeter. This definition of the deformation is reasonable given the convoluted shape that the drop may assume during deformation. On the other hand, this definition does not reflect the orientation of the drop. However, given the emphasis in this study on elongational flow, the drop orientation does not change for a drop moving along the axis of the channel. For a drop moving near the wall, the drop orientation changes with position as will be seen; in this case, the angle of orientation will also be examined. The evolution of the deformation for $0.4 \leq n \leq 1$ is shown in Figure 4. The case $n = 0$ corresponds to a Newtonian drop, and is included for reference. In all cases, $d(t)$ increases, reaches a maximum at the neck, and then decreases as the drop moves toward the exit. The symmetry in the curves reflects the fact that the drop recovers its initial shape as it nears the exit. As expected, deformation is more pronounced for a drop that is more shear thinning.

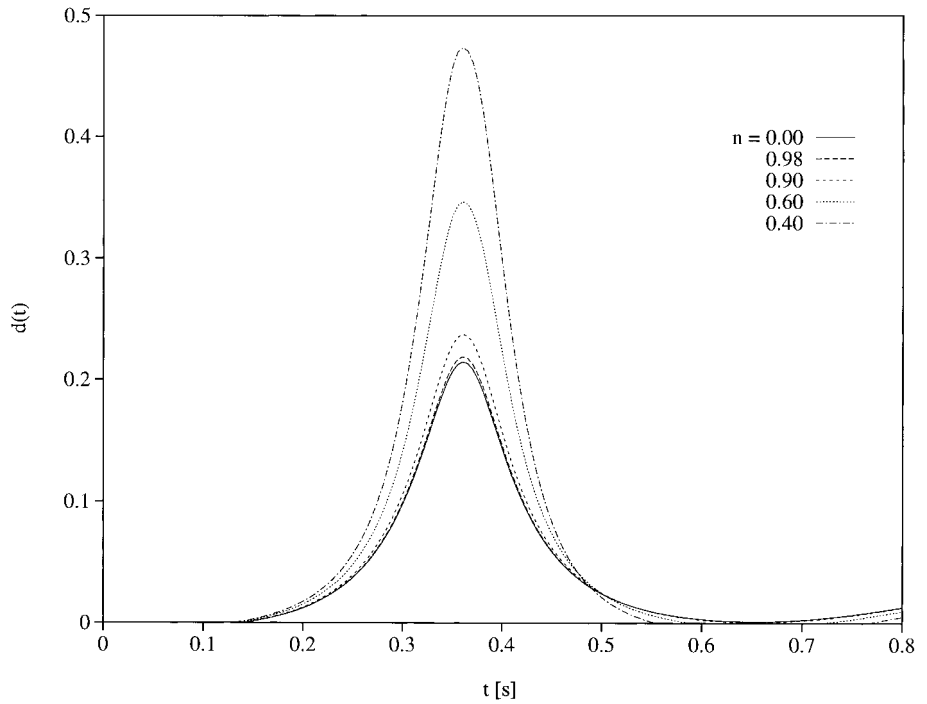

Figure 4. Influence of shear thinning on drop deformation for a drop of initial diameter $D_0 = 0.4$ cm. Evolution of the relative deformation $d(t)$ for five values of the power-law exponent $0.4 \leq n \leq 1$. Note that $n = 1$ corresponds to a Newtonian drop.

The evolution of the viscosity ratio is somewhat more revealing as depicted from Figure 5. The figure displays essentially the evolution of the drop viscosity since η_s is kept constant. Given the maximum in deformation at the neck (Figure 4), one would expect the drop viscosity to be lowest at that point. However, this is the case for drops with weak shear thinning as shown for the case $n = 0.98$. Typically, this is not the case as can be observed from Figure 5. The viscosity reaches a minimum as the drop approaches the neck, but only to go through a maximum and another minimum as the drop exits the neck region. The presence of three extrema is due to the fact that viscosity depends on the rate of strain and not on the deformation itself. This is further inferred by comparing each curve in Figure 4 with its correspondence in Figure 5. As $d(t)$ reaches its maximum, the rate of deformation is (locally) zero, leading to no shear thinning effect. On the other hand, as the rate of deformation is highest on either sides of the maximum, the effect of shear thinning becomes most dominant. This one-to-one correspondence between rate of deformation and shear thinning is fairly easy to detect for a small drop or a drop moving on the axis. In this case the flow around the drop is predominantly elongational as the drop remains far from the walls. For larger drops, the picture becomes more complicated as shear effects become more influential, hence, the importance of examining the interplay between drop size and shear thinning.

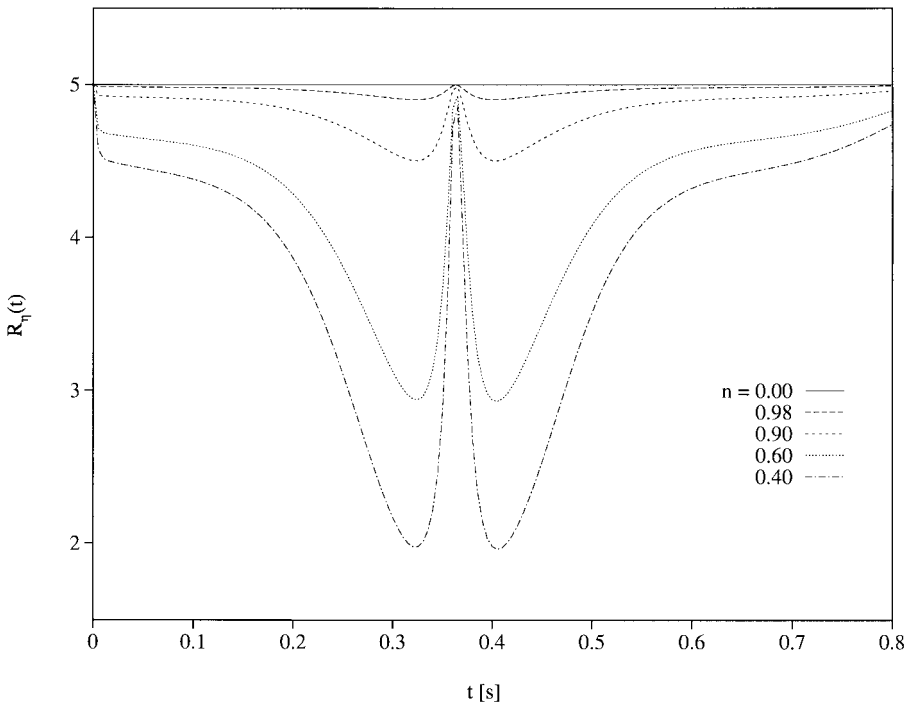

Figure 5. Influence of shear thinning on drop viscosity for a drop of initial diameter $D_0 = 0.4$ cm. Evolution of the drop-to-suspending fluid viscosity ratio $R_\eta(t)$ for five values of the power-law exponent $0.4 \leq n \leq 1$.

3.3. Interplay between drop size and shear thinning

The size of the drop relative to the channel dimensions, particularly the channel width, is a determining factor on the drop deformation. The drop size dictates the relative dominance of shear or elongation of the suspending fluid. Thus, if the drop is large relative to the channel opening, then the influence of shear flow, originating from the channel wall, is significant. If the drop size is relatively small, then the elongational flow dominates. Influence of the shear and elongation flow on the drop deformation is investigated in this section by examining the influence of initial drop diameter D_0. The evolution of $d(t)$ can be plotted against either time or position along the channel axis. The time representation, however, is found to be more revealing as far as the deformation dynamics is concerned.

The influence of drop size on deformation is examined by monitoring the evolution of a drop placed initially on and moving along the channel axis as in Figure 2. The parameters for the drop(s) are the same as before except the size(s) of the drop(s). The evolution of deformation is shown in Figure 6 for $0.4 \leq D_0$ (cm) ≤ 4. The power-law exponent is kept at $n = 0.6$. For a relatively small drop ($D_0 = 0.4$ cm), the deformation increases, reaches a

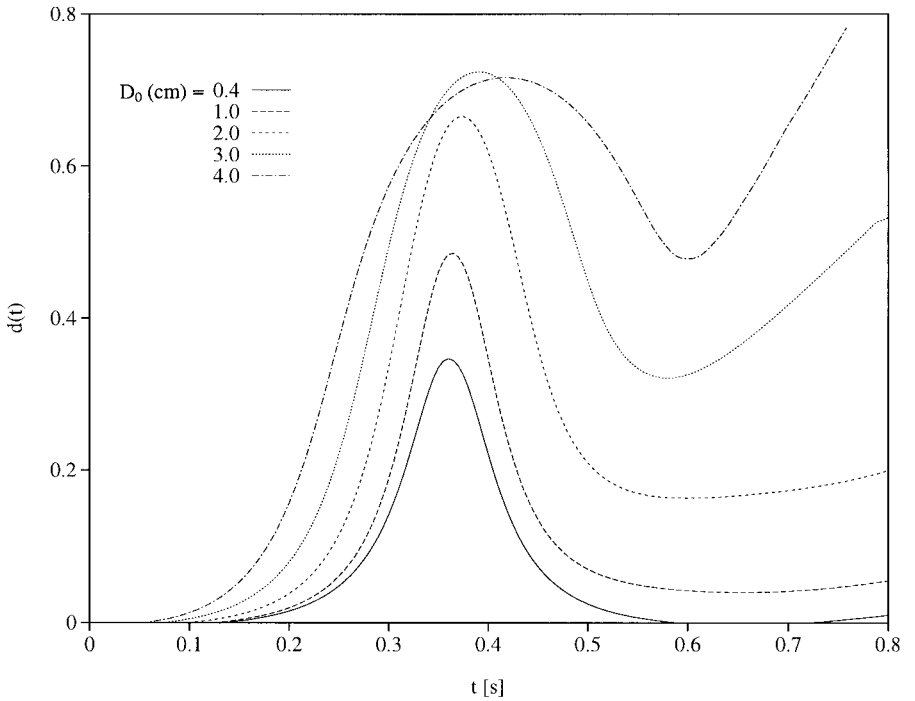

Figure 6. Influence of initial drop size on deformation for $0.4 \leq D_0$ (cm) ≤ 4 and $n = 0.6$. Evolution of the relative deformation $d(t)$ is plotted versus time. Note the symmetry of deformation with respect to neck region.

maximum at the neck, and then decreases as the drop moves toward the exit. In this case, the drop recovers its initial shape as in Figure 2. As the size of the drop increases the symmetry is broken. For a drop of intermediate size [$0.4 < D_0$ (cm) ≤ 2], there is a flattening in $d(t)$ as the drop moves beyond the neck. For a larger drop ($D_0 \geq 3$ cm), the drop deforms significantly as it nears the exit of the channel. In fact, deformation begins to increase indefinitely between the neck and the exit.

The evolution of the corresponding viscosity ratios is shown in Figure 7 for the same range of initial drop diameters. Although the correlation between rate of deformation and viscosity is obvious for small drops, it is not so obvious for larger drops. In the former case, the deformation is essentially elongational, and the direct correlation between the rate of deformation and viscosity can be easily inferred. In the latter case, the drop is large enough for both shear and elongational effects to be present. In general, viscosity is observed to decrease as the rate of deformation increases. This is not the case for drop with ($D_0 \geq 3$ cm), especially when the drop moves between the neck and the exit of the channel. Further insight on the relative predominance of shear and elongation is gained by examining the influence of the initial position of the drop.

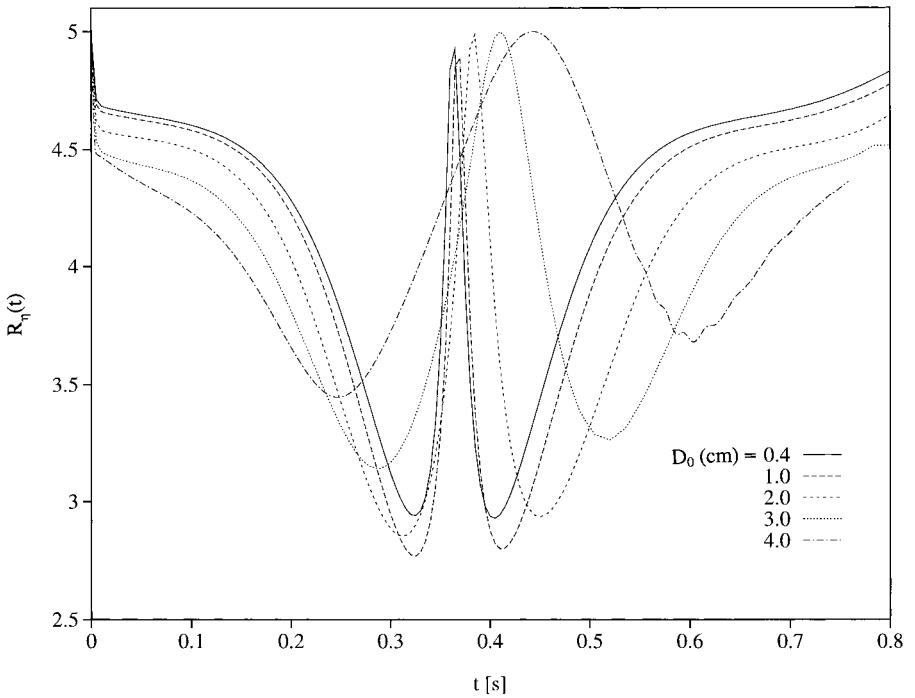

Figure 7. Influence of initial drop size on viscosity ratio for $0.4 \leq D_0$ (cm) ≤ 4 and $n = 0.6$. Evolution of $R_\eta(t)$ is plotted versus time. Note the symmetry of deformation with respect to neck region.

3.4. Interplay between initial position and shear thinning

In this section, the effect of the drop initial position on deformation will be examined. The drop may be initially located either off the channel axis (vertical shift), or on the channel axis at different distances upstream from the neck centre (horizontal shift). Thus, if the drop is initially positioned far from the channel axis, then the influence of shear flow from the channel wall should be significant. While the effect of horizontal shift can somewhat be anticipated, that of the vertical shift is intuitively less obvious. Thus, only the effect of vertical shift is examined here. In order to examine wall effects, the diameter of the drop will be taken smaller than in the previous sections. However, it is helpful to begin this section with a relatively large drop. A more detailed discussion will be given for the smaller drop.

Consider then the deformation of a drop of initial diameter $D_0 = 0.4$ cm. The power-law exponent is fixed again at $n = 0.6$. The evolution of the deformation is shown in Figure 8 and that of the viscosity ratio is displayed in Figure 9 for four drops, # 1, 2, 3 and 4, initially located at $Y_0 = 7$, 6.7, 6.5 and 6 cm respectively. The case of drop # 1 has already been studied, and is included here for reference. Figure 8 shows that a drop, initially located off axis, does not recover its initial shape as it nears the exit of the channel. Instead, the drop reaches maximum deformation at the neck but remains deformed to a degree that increases

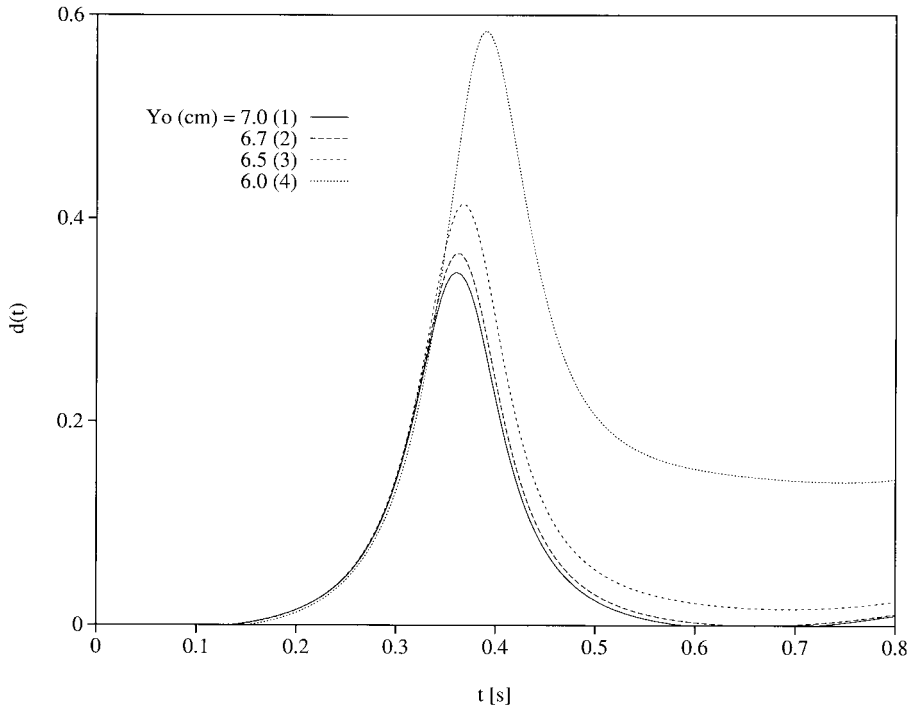

Figure 8. Influence of initial drop position on deformation for a drop of initial diameter $D_0 = 0.4$ cm and $n = 0.6$. Evolution of the relative deformation $d(t)$ is plotted versus time for four initial positions $Y_0 = 7$, 6.7, 6.5 and 6 cm.

with shear thinning. The evolution of the viscosity cannot be entirely inferred from the rate of deformation. This is depicted form Figure 9 for drops # 2–4. Despite the presence of a maximum in $d(t)$, which reflects zero rate of deformation, the drop viscosity does not always recover the Newtonian (zero rate of strain) limit. For a drop moving relatively far from the axis, as the case of # 4, the viscosity reaches a minimum at the neck and then increases monotonically.

To assess further the influence of the initial position, a smaller drop ($D_0 = 0.2$ cm) is now considered. In this case, the drop is allowed to approach the wall closer than previously. As a general rule, in order to avoid error accumulation, the distance between drop and wall should not be below the local mesh size. In what follows, only the evolution of three drops # 1, 2 and 3 will be monitored. The initial distance from the channel axis varies from zero ($Y_0 = 7$ cm) for drop # 1 to 2.5 cm ($Y_0 = 4.5$ cm) for drop # 3. The deformation of drop # 1 has already been presented above and is taken as reference. In order to assess more clearly the effect of shear thinning, it is instructive to discuss first the case of Newtonian drops. So consider the deformation of drops with constant viscosity ratio: $R_\eta(t) = 10$. The results are shown in Figure

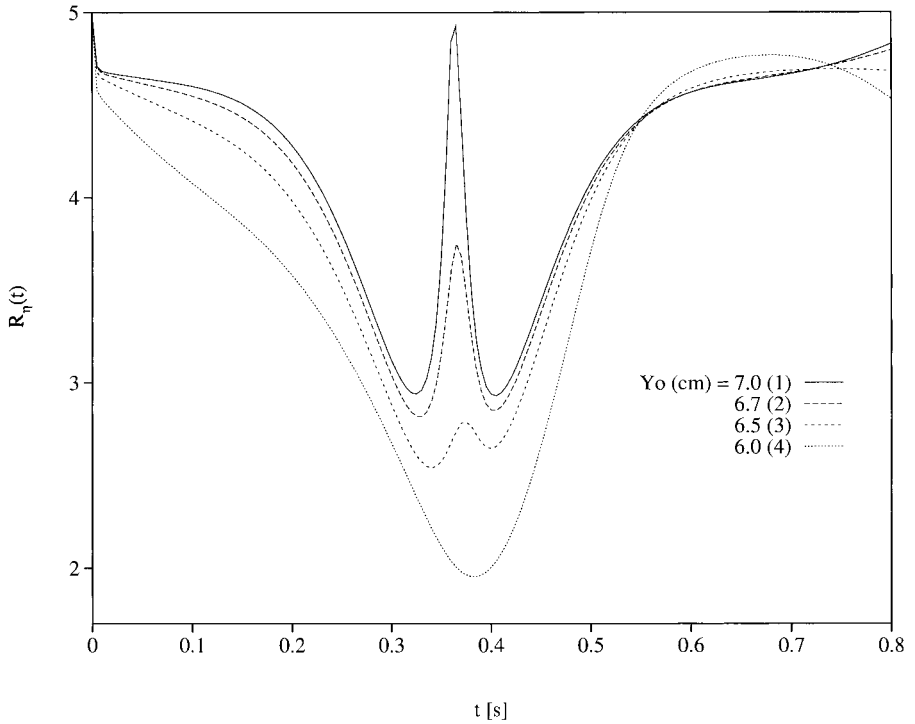

Figure 9. Influence of initial drop size on viscosity ratio for a drop of initial diameter $D_0 = 0.4$ cm and $n = 0.6$. Evolution of $R_\eta(t)$ is plotted versus time for four initial positions $Y_0 = 7$, 6.7, 6.5 and 6 cm.

10. The evolution of the drop shape for each initial position, the corresponding deformation and the angle of orientation for each case are shown in Figure 10(a), (b) and (c) respectively.

As Figure 10(a) and (b) indicate, the initial vertical displacement of the drop influences the rate and the magnitude of drop deformation. Thus, drop # 2 deforms similar to drop # 1 but at a slower pace. As the drop reaches the neck region and approaches the channel axis, it stretches slightly more than drop # 1. Furthermore, in the convergent part of the channel, drop # 2 tends to be dragged away from the channel wall toward the channel axis. As the drop comes out of the neck region, it is swept back into the region near the wall, where similar to drop # 1 it recovers its initial shape. For drop # 3, the deformation is still slower and larger than that of drop # 2. In the divergent zone, the drop begins to recover some of its circular shape but eventually stretches again as it heads towards the exit. At this point, in contrast to drop # 1, drops # 2 and # 3 remain significantly stretched and never recover their initial shape. More importantly, the number of extrema in $d(t)$ increases with initial drop distance from the channel axis. There is even a significant decrease in the first maximum, which occurs before the drop reaches the neck of the channel. The reason for this decrease is the tumbling motion of the drop; its compression within the convergent part of the channel

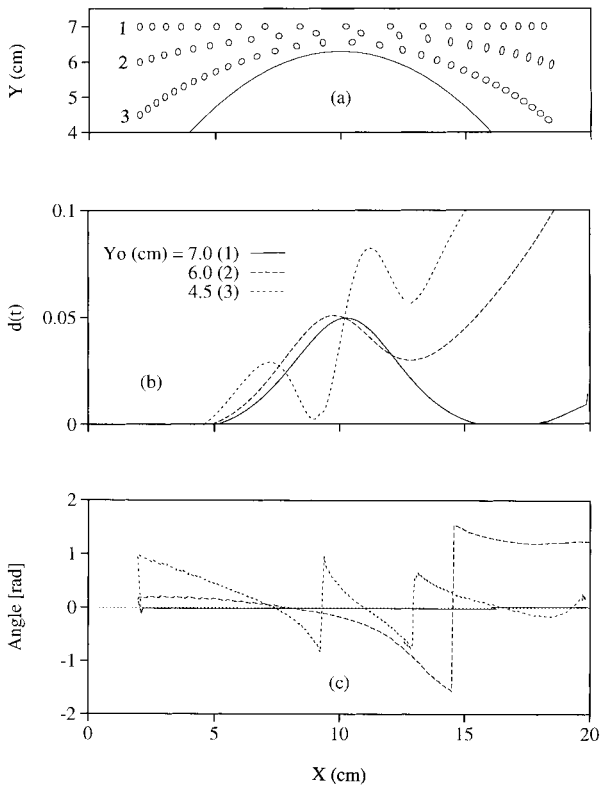

Figure 10. Influence of initial position for Newtonian drops # 1, # 2 and # 3, located off the channel axis by distances: 0, 1 and 2.5 cm ($Y_0 = 7$, 6 and 4.5 cm) respectively. The size of the drops is $D_0 = 0.2$ cm and $R_\eta = 10$. Drop deformation along the channel is shown in (a). Evolution of the relative deformation $d(t)$ is plotted in (b). The orientation of the drop is shown in (c). The horizontal scale (along the channel axis) is taken the same for the three parts.

stifles the stretching before the expected maximum deformation in the neck region could take place. However, as the tumbling slows down within the divergent part of the channel, the drop becomes subjected to further extension.

The tumbling motion is best illustrated by monitoring the evolution of the orientation of the drop; more particularly, the angle that the drop major axis makes with the horizontal (axis). The evolution of the orientation angle, $a(t)$, is shown in Figure 10(c). Obviously, the drop has no orientation initially, and $a(t = 0)$ is taken equal to zero. The figure shows that drop # 1 remains essentially oriented in the same direction; it does not rotate as it is moving along the axis. In contrast, drop # 2 experiences some 'instantaneous' orientation initially, with $a(t = 0) > 0$, and the angle of orientation decreases with motion until it vanishes before deformation is maximum. At this point, the drop reorients itself parallel to the channel axis. This decrease in $a(t)$ continues until $a = -\pi/2$, when the drop is perpendicular to the axis, just before

deformation reaches a minimum. As the drop moves toward the exit the drop is again parallel to the channel axis. For drop # 3 the shear flow component is greater than that for drop # 2. Its main effect is the generation of a tumbling motion of the slightly elongated drop that repeatedly stretches and compresses it during the flow through the channel. The drop undergoes two periods of rotation. Thus, for relatively large viscosity ratios, shearing has a minor influence on the drop deformation; its main effect being the generation of a tumbling motion of slightly deformed particles. This phenomenon is considerably diminished when shear thinning is present.

The situation for a shear-thinning drop is depicted in Figure 11, which shows a significant increase in drop deformation for a drop moving closer to the wall (drop # 3). This is expected since the viscosity decreases significantly for drop # 3 due to shear effect. Unlike the case for Newtonian drops (Figure 10), an initial vertical shift does not always enhance tumbling of the

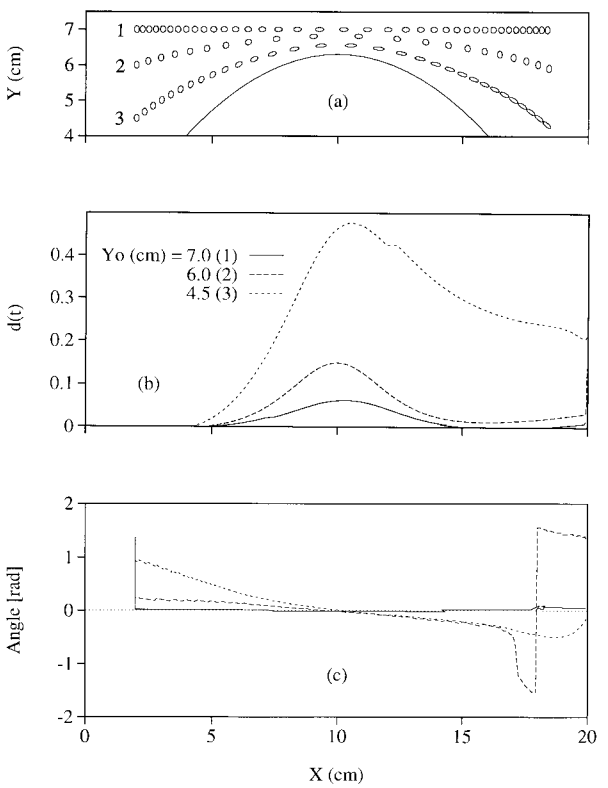

Figure 11. Influence of initial position for shear-thinning drops # 1, # 2 and # 3, located off the channel axis by distances: 0, 1 and 2.5 cm ($Y_0 = 7$, 6 and 4.5 cm) respectively. The size of the drops is $D_0 = 0.2$ cm and the Newtonian drop-to-matrix viscosity ratio is 10. Drop deformation along the channel is shown in (a). Evolution of the relative deformation $d(t)$ is plotted in (b). The orientation of the drop is shown in (c). The horizontal scale (along the channel axis) is taken the same for the three parts.

drop. This is best illustrated by comparing the motions of drop # 2 and drop # 3 in Figure 11 (note that drop # 1 behaves similar to a Newtonian drop). Figure 11(a) and (c) indicate that drop # 2 undergoes at least one period of rotation while drop # 3 rotates less. As established above, rotation is the result of stretching followed by compression. In this case, the presence of shear thinning tends to prohibit compression and enhances stretching. As a result, the drop (here # 3) tends to align itself with the axis while undergoing significant deformation. More importantly, while shear effects are inefficient for droplet deformation (and eventually break-up and dispersion) relative to elongational effects, they may become the dominant mechanism for droplet dispersion for non-Newtonian drops.

4. DISCUSSION AND CONCLUSION

The influence of shear thinning for a drop deforming in a convergent–divergent channel is examined using a generalized BEM for the Carreau–Bird viscosity model. A boundary-only formulation is proposed, which accounts for the non-linearity stemming from the dependence of drop viscosity on the rate-of-strain tensor. At each time step, the viscosity is assumed to be uniform over the drop region. The viscosity is evaluated based on the magnitude of a rate-of-strain averaged over the drop. The extent to which this approximation is valid is of course of crucial importance. The uniformity of rate-of-strain and, consequently, of viscosity cannot obviously be expected to hold, though approximately, for any flow configuration. The approximation ceases to be valid for drops that are large relative to the confining dimensions, or under a flow with significant shearing. However, it is now argued that the validity of the approximation holds reasonably well for a large class of extensional flow, such as convergent–divergent flows. Several cases were examined in this study but the situation can be typically illustrated by the deformation of a small drop moving along the channel axis.

The error in the approximation of viscosity is monitored by comparing the average value with the local value along the interface. It is found that the magnitude of the rate of strain is generally not constant along the interface, at any stage of the deformation. However, the variation in viscosity is not significant. The present discussion is restricted to a drop of initial radius of 0.1 cm, initial viscosity ratio $R_\eta^0 = 5$, and power-law exponent $n = 0.6$. Figure 12 displays the dependence of the viscosity on arc length, s, along the interface. The origin is taken to coincide with the head of the drop. The figure displays the viscosity ratio at different stages of deformation along the channel. At each stage of deformation the viscosity is clearly not uniform, but the variation is generally found to be within a few per cent. At the earlier stages of deformation (Figure 12(a)), the viscosity is highest at the lateral sides of the drop ($s = 0.16$ and 0.47 cm) and is smallest at the head ($s = 0$) and tail ($s = 0.31$ cm). Thus, and as expected, the magnitude of the rate of strain is relatively insignificant at the lateral sides since little shear flow develops there due to the continuity of flow at the interface. As the drop moves towards the neck region, Figure 12(b) indicates the emergence of a relatively strong and localized shear thinning effect that develops at the head of the drop. Right before the drop reaches the neck, the viscosity increases sharply anywhere along the interface, particularly at the tail of the drop. This clearly indicates that shear thinning is essentially absent as the drop

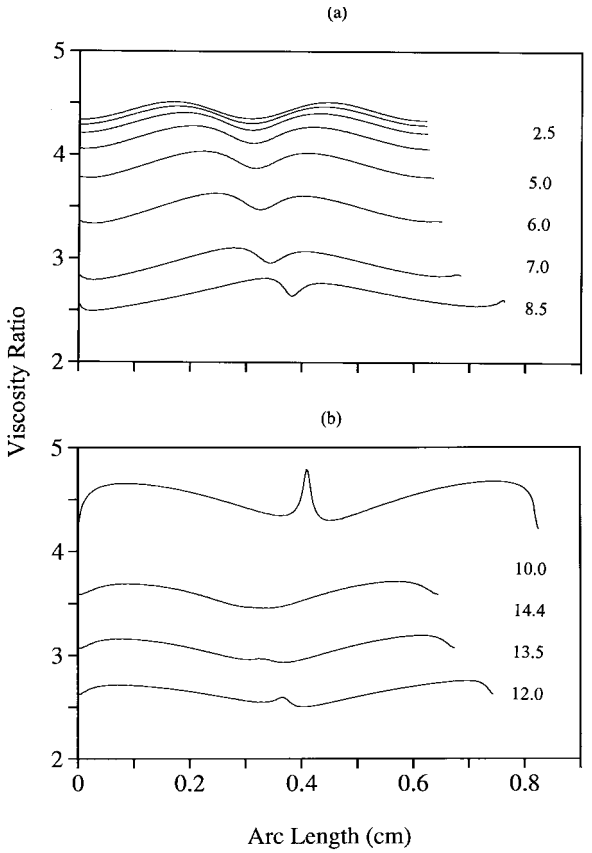

Figure 12. Variation of viscosity ratio along the interface between drop and suspending fluid for a drop moving along the channel axis. The figure shows the dependence of viscosity on arc length for different positions of the drop along the channel axis. The initial viscosity ratio R_η^0 is equal to 5, the drop radius is 0.1 cm and $n = 0.6$. The stages corresponding to $X \in [2.5, 8.5]$ cm are shown in (a) and those to $X \in [10, 14.4]$ cm are shown in (b).

undergoes pronounced elongation. The viscosity decreases and becomes relatively uniform again as the drop emerges out of the neck region.

A more accurate assessment of the error involved is achieved by plotting the maximum and minimum of the viscosity along the interface against the position of the drop. This dependence is shown in Figure 13, along with the approximated (averaged) value of the viscosity at each position. The figure indicates clearly that the averaged viscosity behaves similar to the maximum and minimum viscosities. The approximate viscosity is generally overestimated in the convergent (and divergent) region(s) of the channel. As the drop approaches the neck ($X = 10$ cm) the viscosity begins to increase, reaching essentially the Newtonian level. In the vicinity of the neck (before and after), the approximate viscosity is practically the same as the

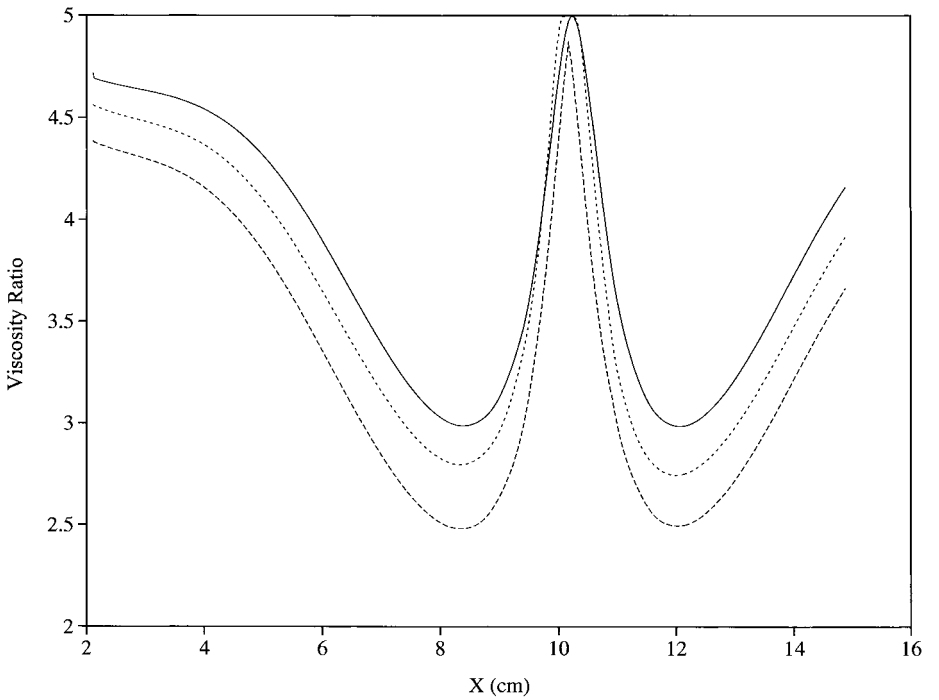

Figure 13. Variation of viscosity ratio with time. The figure shows the evolution of the averaged viscosity ratio $R_\eta(t)$ (—), the maximum (– – –) and the minimum viscosity (- - -) ratio along the drop interface. The initial viscosity ratio is equal to $R_\eta^0 = 5$, the drop radius is 0.1 cm and $n = 0.6$.

local value. It is concluded that the behaviour, as well as the value of the approximated viscosity, follows closely the behaviour and the value of the viscosity along the interface. The approximation is accurate in the neck region, where elongational effects are dominant and shearing is relatively weak. Even far away from the neck region, where shear thinning effects are relatively strong, the approximation of averaged viscosity is reasonable.

The results in the present study are limited to relatively simple configurations. However, the methodology and formulation proposed are not restricted to such simple configurations. They can be easily extended to drops deforming in more complex flows, such as inside single- and twin-screw extruders [6], possibly involving more than one drop. The method is also potentially applicable for larger continuous media that exhibit shear thinning. In this case, the medium may be subdivided into subdomains over which the rate of strain is averaged out to estimate the local viscosity. This approach is of course reminiscent of the implementation of the BEM to composite domains. A word of caution is, however, in order. An averaged strain rate cannot possibly be reflective of the true behaviour if the local variation in the velocity gradient is significant. Another alternative is to take an averaged viscosity rather that an averaged rate of strain over the drop. Rough estimates based on the results in Figures 12 and 13 indicate the

two approaches would not yield significantly different results. Moreover, calculating locally the viscosity and taking the average over the drop region is a costlier alternative as the rate of strain must be calculated at a number of points in the drop, which is not directly available from the BEM. In this case, discretization of the drop region is needed (similarly to the FEM) to compute velocity gradients. The proposed approach circumvents all these difficulties.

In summary, the effects of shear and elongation on the drop deformation are investigated by examining the effects of material properties and geometry of the drop-matrix system. Such effects include the drop size, viscosity ratio and initial position of the drop relative to the channel axis (vertical shift). Other influencing parameters such as interfacial tension, channel convergence, horizontal shift, flow rate and fluid elasticity have already been investigated previously [4–6]. Although the effect of shear thinning is accounted for approximately, the formulation leads to physically realistic results. It is found, for instance, that for a given flow system, the deformation of a drop placed on the channel axis is smaller for smaller initial drop diameter. Furthermore, for a relatively large drop there is a loss of shape recovery (symmetry), caused by the low elongation in the neck region, accompanied by shearing of the outer regions of the drop—shear effects are more important for the larger drops. The initial vertical displacement of the drop relative to the channel axis influences the rate and magnitude of drop deformation. However, these effects are strongly affected by (the zero shear rate) viscosity ratio and shear thinning. For low values of $R_\eta^0 \leq 4$, the shear flow increases the drop residence time in the channel, what in turn enhances the total deformation. For higher values of R_η^0, the drops showed little deformation, tumbling along the channel, and being alternatively stretched or compressed. In this case, shear thinning tends to enhance deformation, prohibiting drop rotation.

Finally, there are a number of issues that need to be addressed further. Specifically, is the averaged rate of strain approach extensible to other geometries and flows where the effects of shear and/or extension may be significantly larger than in the present work? The general answer to this question may very well be inferred from the current results: the approximate approach is valid under conditions of relative dominance of extensional flow. Other issues, such as the approximate inlet and outlet boundary conditions, the mesh size at the interface, the type of boundary element, the need for adaptive meshing, also need to be addressed more closely. Some of these issues have already been or are being currently examined [14].

ACKNOWLEDGMENTS

This work is supported by the Natural Sciences and Engineering Council of Canada.

REFERENCES

1. Grace HP. *Third Engineering Foundation Research Conference on Mixing*. Andover, NH, 9–14 August 1971.
2. Rallison JM. The deformation of small viscous drops and bubbles in shear flows. *Annual Review in Fluid Mechanics* 1984; **16**: 45.
3. Stone HA. Dynamics of drop deformation and breakup in viscous fluids. *Annual Review in Fluid Mechanics* 1994; **26**: 65.
4. Khayat RE, Luciani A, Utracki LA. Boundary-element analysis of planar drop deformation in confined flow. Part I. Newtonian fluids. *Engineering Analysis of Boundary Elements* 1997; **19**: 279.

5. Khayat RE, Huneault MA, Utracki LA, Duquette R. Boundary element analysis of planar drop deformation in the overflight region of a twin-screw extruder. *Engineering Analysis of Bound Elements* 1998; **21**: 155.
6. Khayat RE, Luciani A, Utracki LA. Boundary-element analysis of planar drop deformation in confined flow. Part II. Viscoelasic fluids. *Engineering Analysis of Boundary Elements* 1998; **22**: 291.
7. Khayat RE, Luciani A, Utracki LA, Godbille F, Picot J. Influence of shear and elongation on drop deformation in convergent/divergent flow. *International Journal of Multiphase Flow* 2000; **26**: 17.
8. Bourry D, Godbille F, Khayat RE, Luciani A, Picot J, Utracki LA. Extensional flow of polymeric dispersions. *Polymer Engineering Science* 1999; **39**: 1072.
9. Khayat RE, Derdouri A, Hebert LP. A boundary-element approach to three-dimensional gas-assisted injection molding. *Journal of Non-Newtonian Fluid Mechanics* 1995; **57**: 253.
10. Khayat RE, Raducanu P. A coupled finite element/boundary element approach for the three-dimensional simulation of air venting in blow molding and thermoforming. *International Journal for Numerical Methods in Engineering* 1998; **43**: 151.
11. Khayat RE, Derdouri A, Frayce D. Boundary-element analysis of three-dimensional transient mixing processes of Newtonian and viscoelastic fluids. *International Journal for Numerical Methods in Fluids* 1998; **28**: 815.
12. Khayat RE. A boundary-element analysis of 3D multiply-connected cavity mixing of polymer solutions. *International Journal for Numerical Methods in Fluids* 1999; **31**: 1173.
13. Khayat RE. A three-dimensional boundary-element approach to confined potential free-surface flow as applied to die casting. *Engineering Analysis of Boundary Elements* 1998; **22**: 83.
14. Khayat RE, Marec K. An adaptive boundary-element Lagrangian approach to 3D transient free-surface flow of viscous fluids. *Engineering Analysis of Boundary Elements* 1999; **23**: 111.
15. Floryan JM, Rasmussen H. Numerical methods for viscous flows with moving boundaries. *Applied Mechanics Reviews* 1989; **42**: 323.
16. Bird RB, Armstrong RC, Hassager O. *Dynamics of Polymeric Liquids* (2nd edn), vol. 1. Wiley: New York, 1987.
17. Tran-Cong T, Phan-Thien N. Three-dimensional study of extrusion processes by boundary element method. II. Extrusion of a viscoelastic fluid. *Rheology Acta* 1988; **27**: 639.
18. Tanner RI. *Engineering Rheology*. Oxford University Press: Oxford, 1988.
19. Bush MB, Tanner RI, Phan-Thien N. A boundary element investigation of extrudate swell. *Journal of Non-Newtonian Fluid Mechanics* 1985; **18**: 143.
20. Coleman CJ. On the use of boundary integral methods in the analysis of non-Newtonian fluid flow. *Journal of Non-Newtonian Fluid Mechanics* 1984; **16**: 347.
21. Wrobel LC. The dual reciprocity boundary element formulation for nonlinear problems. *Computational Methods and Applications in Mechanical Engineering* 1987; **65**: 147.
22. Nowak AJ. Application of the multiple reciprocity method for solving nonlinear problems. In *Advanced Computational Methods in Heat Transfer II*, *Vol I: Conduction*, *Radiation and Phase Change*, Wrobel LC, Brebbia CA, Nowak AJ (eds). Computational Mechanics Publications: Southampton, 1995.
23. Neves AC, Brebbia CA. The multiple reciprocity boundary element method for transforming domain integrals to the boundary. *International Journal for Numerical Methods in Engineering* 1991; **31**: 709.
24. Power H, Wrobel LC. *Boundary Integral Methods in Fluid Mechanics*. Computational Mechanics Publications: Southampton, 1995.
25. Frayce D, Khayat RE. A dual reciprocity boundary element approach to three-dimensional transient heat conduction as applied to materials processing. *Numerical Heat Transfer A* 1996; **29**: 243.
26. Toose EM, Geurts BJ, Kuerten JGM. A boundary integral method for two-dimensional (non)-Newtonian drops in slow viscous flow. *Journal of Non-Newtonian Fluid Mechanics* 1995; **60**: 129.
27. Toose EM, Van den Ende J, Geurts BJ, Kuerten JGM. Axisymmetric non-Newtonian drops treated with a boundary integral method. *Journal of Engineering in Mathematics* 1996; **30**: 131.

